Electrically driven spin excitation in the ferroelectric magnet DyMnO₃

N. Kida,[1] Y. Ikebe,[2] Y. Takahashi,[1] J. P. He,[1] Y. Kaneko,[1] Y. Yamasaki,[3] R. Shimano,[1,2] T. Arima,[4]
N. Nagaosa,[3,5] and Y. Tokura[1,3,5]

[1]*Multiferroics Project (MF), ERATO, Japan Science and Technology Agency (JST), c/o Department of Applied Physics,*
The University of Tokyo, 7-3-1 Hongo, Bunkyo-ku, Tokyo 113-8656, Japan
[2]*Department of Physics, The University of Tokyo, 7-3-1 Hongo, Bunkyo-ku, Tokyo 113-0033, Japan*
[3]*Department of Applied Physics, The University of Tokyo, 7-3-1 Hongo, Bunkyo-ku, Tokyo 113-8656, Japan*
[4]*Institute of Multidisciplinary Research for Advanced Materials, Tohoku University, 2-1-1 Katahira, Aoba-ku, Sendai 980-8577, Japan*
[5]*Cross-Correlated Materials Research Group (CMRG), ASI, RIKEN, 2-1 Hirosawa, Wako, 351-0198, Japan*
(Received 4 July 2008; published 18 September 2008)

Temperature (5–250 K) and magnetic-field (0–70 kOe) variations of the low-energy (1–10 meV) electrodynamics of spin excitations have been investigated for a complete set of light-polarization configurations for a ferroelectric magnet DyMnO₃ by using terahertz time-domain spectroscopy. We identify the pronounced absorption continuum (1–8 meV) with a peak feature around 2 meV, which is electric-dipole active only for the light E vector along the a axis. This absorption band grows in intensity with lowering temperature from the spin-collinear paraelectric phase above the ferroelectric transition but is independent of the orientation of spiral spin plane (bc or ab), as shown on the original P_s (ferroelectric polarization) ∥c phase as well as the magnetic-field induced P_s∥a phase. The possible origin of this electric-dipole active band is argued in terms of the large fluctuations of spins and spin current.

I. INTRODUCTION

The magnetoelectric (ME) effect, in which the electric polarization can be induced by a magnetic field H or the magnetization can be induced by an electric field E, has been known since the 1950s.[1] However, the materials showing the large ME effect are rare. Recently, the interest has been revived by the observation of the ferroelectric polarization P_s and its 90° flop in the presence of a finite field H (Ref. [2]) in orthorhombically distorted perovskite manganites, RMnO₃, where R represents Tb, Dy, and Gd ions.[2–4] In DyMnO₃, for example, the collinear spin order of Mn ions sets in at the Néel temperature T_N^{Mn} of 39 K with the incommensurate (IC) modulation vector $q_b^{Mn} \sim 0.36$ along the b axis.[3] Noticeably, the ferroelectricity shows up along the c axis when the transverse bc spiral (cycloidal) spin order[5] evolves below T_c of 19 K. The direction of P_s is flopped to the a axis when H is applied along the b axis.[3,4] So far, a wide variety of the ferroelectric magnets, termed multiferroics, have been found in a family of cycloidal-spin magnets.[1] The ferroelectricity in RMnO₃ can be microscopically explained by the spin-current model[6] or equivalently by the inverse Dzyaloshinski-Moriya effect,[7,8] as expressed by the relation, $P_s \propto e_{ij} \times (S_i \times S_j)$, where e_{ij} is the unit vector connecting i and j sites. Namely, the cycloidal spin structure can induce the ferroelectricity along the direction perpendicular to the modulation vector and within the spiral spin plane. A direct evidence for this mechanism was recently demonstrated by controlling the vector chirality $(S_i \times S_j)$ of TbMnO₃ with E.[9]

In the magnetically induced ferroelectric phase, the strong ME coupling would also produce the intriguing low-lying optical excitation. In RMnO₃, there are experimental (Ref. [10]) and theoretical[11,12] arguments on the possibility of the presence of the low-lying spin excitation, called *electromagnon*, which is activated electrically. Far-infrared spectros-

copy has provided the useful information for the electrodynamics of TbMnO₃,[10] GdMnO₃,[10,13] and Eu$_{1-x}$Y$_x$MnO₃,[14,15] revealing that an additional light absorption contribution indeed emerges in the ferroelectric phase at terahertz frequencies below the optical-phonon frequencies of the perovskite structure. Among a family of RMnO₃, DyMnO₃ shows the largest ME response; the change in the dielectric constant upon the P_s flop exceeds 500%, and P_s reaches 2 mC/m².[3,4] Therefore, DyMnO₃ offers a good opportunity to clarify the low-energy electrodynamics coupled with the spin excitation.

Here we report on a complete set of optical spectra at terahertz frequencies of a multiferroic DyMnO₃ with varying the light polarization (both the electric-field E^ω and magnetic-field H^ω components of light), temperature T, and applied H, to unravel the strongly electric-dipole allowed spin excitation. The observed excitation is confirmed to be active mainly for $E^\omega \| a$ and not to be correlated with the direction of the spiral spin plane. We focus on spectral signatures, being highly sensitive to the light polarization, in a variety of ME phases that can be tuned by both T and H. The format of this paper is as follows: In Sec. II we describe the detail of the experimental procedure for measurements of terahertz time-domain spectroscopy. Section III is devoted to the optical investigations of the low-energy spin dynamics in a variety of ME phases of DyMnO₃, in which we clarify the unique selection rule of the spin excitation driven by E^ω or H^ω by measurements of the light polarization (Sec. III A), T (Sec. III B), and H (Sec. III C) dependences. On the basis of the results of Sec. III, the origin of the electrically driven spin excitation observed at terahertz frequencies in DyMnO₃ is discussed in Sec. IV. The summary of this paper is given in Sec. V. We also describe in Appendixes the estimation procedure of the complex optical constants from the raw data obtained by terahertz time-domain spectroscopy.
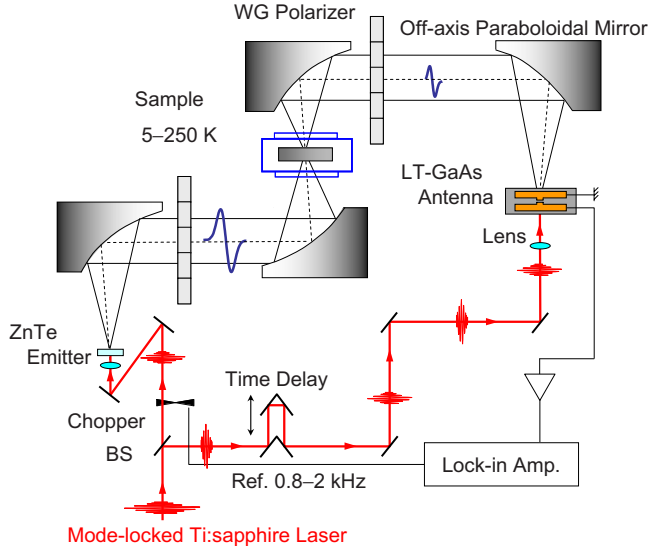
FIG. 1. (Color online) Schematic illustration of the experimental setup for terahertz time-domain spectroscopy in a transmission geometry.

II. METHODS

A. Sample preparation and characterization

The large single crystals of $DyMnO_3$ were grown by a floating zone method. The available ac, ab, and bc surfaces of the crystals with a typical sample size of $4-16$ mm^2 were cut from the ingot by using a back Laue photograph. The respective samples were polished to thickness of $150-800$ μm. The polishing procedure frequently induces the damage on the surface for the case of the orthorhombically distorted perovskite manganites. We confirmed that the optical response was almost unchanged before and after polishing procedure.

The samples cut from the same ingot used in this work were characterized by the measurements of the dielectric constant at low-frequencies as functions of T and H. The ferroelectricity along the c axis in zero H and the P_s flop from the c to a axes in H were clearly observed around 19 K and 20 kOe at 7 K, respectively. The obtained phase diagrams in a plane of T and H are consistent with the previously reported one of $DyMnO_3$.[4]

B. Setup for terahertz time-domain spectroscopy

We used the terahertz time-domain spectroscopy in a transmission geometry to obtain complex refractive index $\tilde{n}$ without using Kramers-Kronig (KK) analysis.[16,17] Terahertz time-domain spectroscopy can easily access the low-energy electrodynamics in solids, typical frequencies from 0.1 to 3 THz.[16] The lower limit of the measurable frequencies depends on the size of the samples since 0.1 THz corresponds to 3 mm in wavelength. We adopted a transmission geometry and the sample was attached to the perforated Cu holder with a diameter of 2, 2.8, 3, and 3.5 mm, which was selected to suitably match the size of the samples.

Figure 1 shows the schematic illustration of terahertz time-domain spectroscopy in a transmission geometry in this

study. For the measurements, we used the photoconducting (PC) sampling technique[18] to obtain terahertz radiation pulse. The femtosecond laser pulses delivered from the mode-locked Ti:sapphire laser (center wavelength of 800 nm, pulse width of 90 fs, and repetition rate of 80 MHz) were used as a source. The laser pulses were divided by a beam splitter (BS). One was used as the pump and another was used as the gate. The pump pulses were irradiated on to the ZnTe crystal[19] to induce the optical rectification effect acting as a source of terahertz radiation.[20] The wire grid (WG) polarizers were inserted in between off-axis paraboloidal mirrors to obtain the linear polarization. The polarized terahertz pulse was focused on the sample by off-axis paraboloidal mirrors. The cryostat was placed within the box filled with dry nitrogen to eliminate the absorption of water. The gate pulses were introduced to the low-temperature-grown GaAs (LT-GaAs) photoconducting device coupled with a dipole antenna after the appropriate time delay.[21] The pump pulses were mechanically chopped and the photocurrent induced by the electric field of the terahertz pulse was lock-in detected. Therefore, the induced photocurrent, which depends on both amplitude and phase of terahertz radiation, can be obtained by varying the optical delay line. Further details of our scheme for terahertz generation and detection can be found in Refs. 16 and 18.
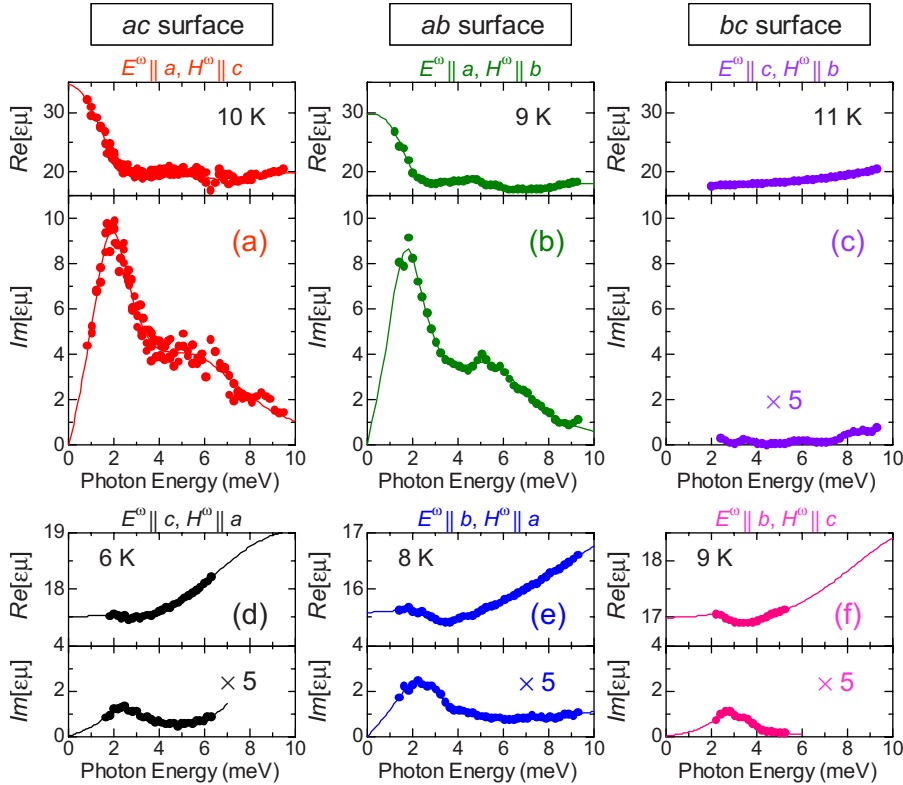
For the measurements of the H dependence, the sample was placed in a cryostat equipped with a superconducting magnet. H supplied from a superconducting magnet was applied along the b axis up to 70 kOe. The measurements in H were mainly performed at 7 K. We adopted a Faraday geometry. Further details of our experimental setup combined with the superconducting magnet can be found in Ref. 22.

Since we consider the spin excitation, which can be driven by either E^ω or H^ω, we numerically estimated $\tilde{n}$ and used the quantity of $\tilde{n}^2 = \epsilon\mu(\omega)$ (not $\tilde{n}^2 = \epsilon$), where ϵ is the complex dielectric constant and μ the complex magnetic permeability. Details of the estimation procedure and the validity of the quantities of $\epsilon\mu$ to characterize the spin excitation are described in Appendixes.

III. RESULTS

A. Light-polarization dependence

First, in Fig. 2, we show $\epsilon\mu$ spectra (closed circles) in the bc spiral spin phase ($P_s \| c$) of $DyMnO_3$ to determine the selection rule with respect to the light polarization, in which E^ω and H^ω were set parallel to the crystallographic axes using available ac, ab, and bc surfaces of the crystal. Upper and lower panels of Fig. 2 present, respectively, the real (Re) and imaginary (Im) parts of $\epsilon\mu$ spectra measured around 10 K with $H=0$. There are remarkable peak structures and noticeable optical anisotropy with respect to E^ω and H^ω. Such a light-polarization dependence, including the negligible absorption for $E^\omega \| c$ and $H^\omega \| b$ [Fig. 2(c)], as well as the conspicuous spectral change around T_c and T_N^{Mn}, cannot be ascribed to the crystalline-electric-field excitation of f electrons, which was reported for $TbMnO_3$ around 4.7 meV by inelastic neutron-scattering studies.[23,24]

FIG. 2. (Color online) Low-energy electrodynamics of a complete set of available configurations of single crystals of DyMnO$_3$ measured around 10 K in zero magnetic field. Upper and lower panels show the real and imaginary parts of $\epsilon\mu$ spectrum (closed circles) when E^ω and H^ω were set parallel to the crystallographic axes of ac, ab, and bc surface crystal plates. The solid lines in (a) and (b) are results of a least-squares fit to reproduce low-lying and high-lying peak structures by assuming two Lorentz oscillators for ϵ. On the contrary, $\epsilon\mu$ spectra in (d), (e), and (f) can be reproduced by two Lorentz oscillators for ϵ and μ as indicated by solid lines.

A broad and pronounced absorption continuum (1–8 meV) overlapped by two peak structures around 2 and 5.5 meV is observed in Im[$\epsilon\mu$] spectrum for $E^\omega\|a$ and $H^\omega\|c$ [lower panel of Fig. 2(a)]. In accord with this, a dispersive structure can be discerned in Re[$\epsilon\mu$] spectrum [upper panel of Fig. 2(a)]. Such a low-lying peak structure was also identified previously at 2.9 meV for TbMnO$_3$,[10] 2.5 meV for GdMnO$_3$,[10,13] and 3 meV for Eu$_{1-x}$Y$_x$MnO$_3$ [Fig. 2(a)] (although this value depends slightly on x).[14,15] Noticeably, Im[$\epsilon\mu$] of DyMnO$_3$ reaches 10 (corresponding to the optical conductivity of about 3 Ω^{-1} cm^{-1}), which is roughly a factor of 2–5 larger than the absorption of TbMnO$_3$ and GdMnO$_3$, suggesting DyMnO$_3$ as the prototype in the study of the low-lying excitation. Such a strong absorption including the spectral shape, peak position, and magnitude was clearly confirmed to be observed only for $E^\omega\|a$ as evidenced by the $\epsilon\mu$ spectra for $E^\omega\|a$ and $H^\omega\|b$ [Fig. 2(b)], i.e., with different H^ω polarization. The low-temperature spectrum can be fitted with two Lorentz oscillators, as indicated by solid lines. The ratio of Re[$\epsilon\mu$] for $E^\omega\|a$ to other configurations was about 2, being consistent with the dielectric constant Re[ϵ] at 10 kHz.[3,4] This indicates the large anisotropy extending up to terahertz frequencies associated with the electric-dipole active excitation.

In Im[$\epsilon\mu$] spectrum for $E^\omega\|c$ and $H^\omega\|a$ [Fig. 2(d)], on the other hand, a broad peak feature is observed where the peak energy nearly matches the low-lying peak energy for $E^\omega\|a$. However, the magnitude of Im[$\epsilon\mu$] in this configuration ($\sim$0.3) is much smaller, by a factor of 30, than the magnitude of Im[$\epsilon\mu$] for $E^\omega\|a$. By comparing the $\epsilon\mu$ spectra for $E^\omega\|c$ and $H^\omega\|a$ [Fig. 2(d)], and $E^\omega\|b$ and $H^\omega\|a$ [Fig. 2(e)], this absorption appears to arise from the $H^\omega\|a$ stimulation in accord with the conventional magnon selection rule for the

bc spiral spin state.[12] We also discern the broad peak feature in $\epsilon\mu$ spectrum for $E^\omega\|b$ and $H^\omega\|c$ [Fig. 2(f)] whose magnitude of Im[$\epsilon\mu$] ($\sim$0.3) is comparable to those of Im[$\epsilon\mu$] ($\sim$0.3–0.5) for cases of $H^\omega\|a$ stimulation. We cannot distinguish the selection rule of this tiny absorption on the basis of the light-polarization dependence alone due to the presence of the intense absorption for $E^\omega\|a$ and $H^\omega\|c$ [Fig. 2(a)]. As will be shown in Sec. III B, however, we identify that this sharp peak structure is also driven by H^ω.

B. Temperature dependence

We present in Fig. 3(b) the T dependence of the selected $\epsilon\mu$ spectra for $H^\omega\|a$. With increasing T, Im[$\epsilon\mu$] tends to decrease in magnitude and the peak position is shifted to the lower energy from 2.8 meV at 5 K to 2 meV at 36 K [lower panel of Fig. 3(b)]. Above T_N^{Mn}, the broad peak structure is diminished, as can be seen in Im[$\epsilon\mu$] spectrum at 50 K (a finite value of Im[$\epsilon\mu$] comes from the absorption tail of the optical phonons). Accordingly, there is no dispersive structure around 2 meV in Re[$\epsilon\mu$] spectrum [upper panel of Fig. 3(b)]. We also show in Fig. 3(c) the selected $\epsilon\mu$ spectra for $H^\omega\|c$ as a function of T. With increasing T, the peak position is also shifted to the lower energy from 3.3 meV at 4.2 K to 2.3 meV at 31 K and the magnitude of Im[$\epsilon\mu$] also tends to decrease. The observed T variation is similar to the case for $H^\omega\|a$; the peak structure seems to vanish above T_N^{Mn} =39 K. Even though we cannot identify the clear signature of the peak structure above 31 K in Im[$\epsilon\mu$] spectrum [lower panel of Fig. 3(c)] due to the detection limit in our experiments ($\sim$1.8 meV), as determined by the size of the sample, there is no signature of the dispersive structure around 2 meV in Re[$\epsilon\mu$] spectrum at 46 K [upper panel of Fig. 3(c)].
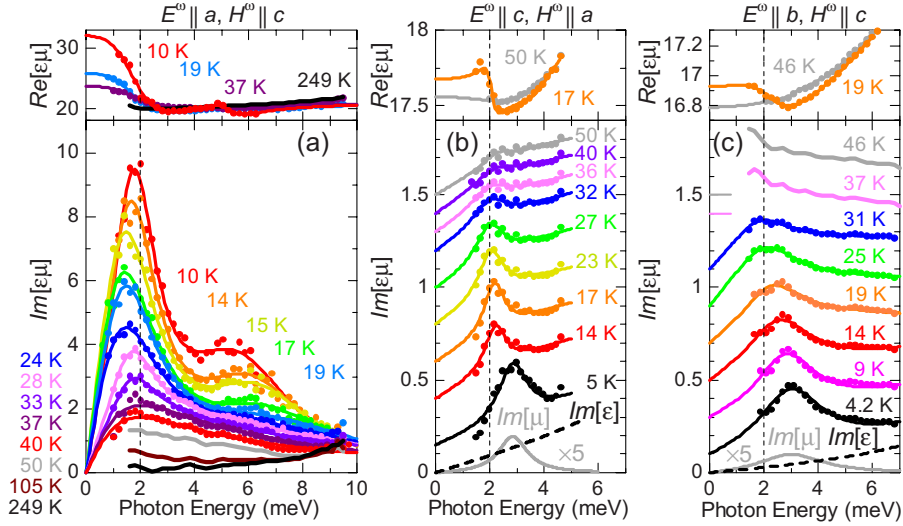
FIG. 3. (Color online) Temperature dependence of the real (upper panels) and imaginary (lower panels) parts of the selected $\epsilon\mu$ spectra (closed circles) of DyMnO$_3$ for (a) $E^\omega\|a$, (b) $H^\omega\|a$, and (c) $H^\omega\|c$. Note that the scale of the vertical axis is different in respective figures. The Im[$\epsilon\mu$] spectra shown in (b) and (c) are vertically offset for clarity. We also plot the extracted Im[ϵ] and Im[μ] spectra [at (b) 5 and (c) 4.2 K] indicated by dotted and gray lines, respectively, by assuming that Im[$\epsilon\mu$] spectrum can be represented by two Lorentz oscillators for ϵ and μ (solid lines). The Im[μ] spectrum is multiplied by 5. On the contrary, $\epsilon\mu$ spectra for $E^\omega\|a$ [(a)] can be fitted by two Lorentz oscillators.

On the basis of the T dependence as well as of the light-polarization dependence presented in Sec. III A, it is reasonable to consider that the observed peak structure can be assigned to the spin excitation of Mn ions driven by $H^\omega\|a$ or $H^\omega\|c$. Indeed, in inelastic neutron-scattering experiments on the bc spiral spin phase of TbMnO$_3$, the magnon dispersion along the [100] or [001] axis comes across $k=0$ around 2 meV.[23,24] To estimate the contribution of the magnon to Im[$\epsilon\mu$] spectrum, we plot in Figs. 3(b) and 3(c) the Im[μ] spectra for $H^\omega\|a$ at 5 K and for $H^\omega\|c$ at 4.2 K, respectively, as indicated by solid lines. These were derived from the relation, Im[$\epsilon\mu$] (=Re[ϵ]Im[μ]+Im[ϵ]Re[μ]) by assuming Lorentz oscillators of ϵ and μ for contributions of phonon (a dotted line) and magnon, respectively.

Next, we show in Fig. 3(a) the T dependence of the $\epsilon\mu$ spectra for $E^\omega\|a$. At 249 K, only the absorption tail due to the optical phonon is observed. With decreasing T but even above T_N^{Mn}, it is clearly discernible that Im[$\epsilon\mu$] in the low-energy region below 8 meV increases and forms a Debye-like absorption band [lower panel of Fig. 3(a)]. In accord with this, the dispersive structure emerges in Re[$\epsilon\mu$] spectrum [upper panel of Fig. 3(a)]. In the collinear phase below T_N^{Mn} (=39 K), a broad peak structure emerges around 2 meV and continuously grows in intensity with further decreasing T. In the bc spiral spin phase below T_c (=19 K), the additional peak structure shows up around 6 meV and its peak position shifts to the lower energy, while the low-lying peak structure shifts to higher energy.

To be more quantitative, we deduced the integrated spectral weight per Mn-site, N_{eff}, as given by

$$N_{eff} = \frac{2m_0V}{\pi e^2}\int_{\omega_1}^{\omega_2}\omega'\,\text{Im}[\epsilon(\omega')\mu(\omega')]d\omega', \qquad (1)$$

where m_0 is the free-electron mass, e the elementary charge, and V the formula (DyMnO$_3$) cell volume. The integrated

energy range was chosen between $\omega_1=0.8$ meV and $\omega_2=9.5$ meV to nearly cover the full band. Figure 4(b) presents T variation of the estimated N_{eff}. We also plotted N_{eff} at 75 (square) and 245 K (triangle) at the 50 K position for clarity. N_{eff} for $E^\omega\|a$ gradually increases below $T_N^{Mn}=39$ K and is sharply enhanced below $T_c=19$ K (indicated by vertical solid lines). This is in contrast to N_{eff} for $H^\omega\|a$ (we adopted $\omega_1=1.5$ meV and $\omega_2=4.6$ meV to estimate N_{eff} of the magnon band), as shown in Fig. 4(a); N_{eff} reaches the maximum at T_c where the bc spiral spin structure evolves from the collinear spin state [note that N_{eff} for $H^\omega\|a$ includes the contribution of the phonon structure, as indicated by a dashed line in Fig. 4(a), which could be crudely estimated with the Im[ϵ] spectrum at 5 K, as indicated by a dotted line in Fig. 3(b)]. The electric-dipole active ($E^\omega\|a$) excitation almost disappears above T_N^{Mn} [Fig. 3(a)], and its energy range (0–10 meV) nearly coincides with that of the magnon band, which was revealed by inelastic neutron-scattering experiments on the bc spiral spin phase of TbMnO$_3$.[23,24] This coincidence of the spectral energy region also ensures that the observed excitation is magnetic in origin.

C. Magnetic-field dependence

As an origin of the electromagnon, the rotational mode of the spiral spin plane around the b axis (propagation vector) has been theoretically proposed based on the spin-current model.[12] This was taken into consideration in the analysis of the inelastic neutron-scattering results for the bc spiral spin phase of TbMnO$_3$ (Ref. 24), and the observed dispersion relation (2.4 meV at $k=0$) was assigned to the rotational mode of the bc spiral spin plane. These apparently contradict the results of ϵ spectra of GdMnO$_3$,[10,13] in which the peak structure with Im[ϵ]$\sim$1 comparable to Im[ϵ] of TbMnO$_3$ was also identified in the IC spin-collinear paraelectric phase. In the course of the P_s flop from the c to a axis at
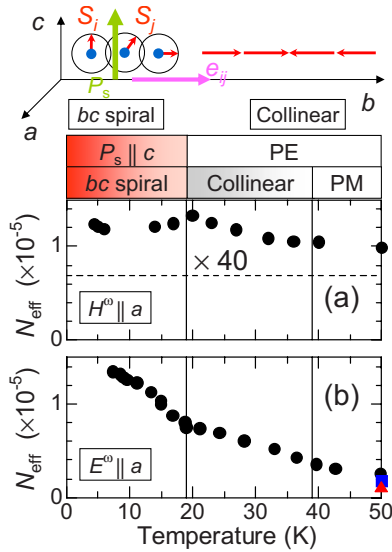
FIG. 4. (Color online) Temperature (T) dependence of the integrated spectral weight per Mn-site, N_{eff}, as defined by Eq. (1) in the text of the ac surface crystal plate of DyMnO$_3$ for (a) $H^\omega \| a$ and (b) $E^\omega \| a$. The upper panel of (a) shows the phase diagram with variation of T. PE and PM stand for paraelectric and paramagnetic, respectively. We also show the schematic illustrations of the bc spiral and collinear spin states induced by T. Néel temperature T_N^{Mn} (39 K) and ferroelectric transition temperature T_c (19 K) are indicated by vertical solid lines in (a) and (b). The data measured at 75 and 249 K were also plotted at the 50 K position in (b) with square and triangle symbols, respectively. The horizontal dashed line in (a) represents the estimated contribution of the optical-phonon absorption at 5 K.

$H_c \sim 20$ kOe, IC q_b^{Mn} (~ 0.37) is kept nearly constant for DyMnO$_3$,[25] as contrasted by the IC to commensurate transition for TbMnO$_3$.[26] Therefore, the measurements of the effect of H on $\epsilon\mu$ spectra of DyMnO$_3$ can provide further insights into the nature of the electromagnon.

The upper and lower panels of Fig. 5(a) present the selected Re[$\epsilon\mu$] and Im[$\epsilon\mu$] spectra for $E^\omega \| a$, measured at 7 K for varying H with $H \| b$ axis, respectively. The experimental setup with use of a superconducting magnet (up to 70 kOe) restricted the measured energy range, and thus we concentrated on the behavior of $\epsilon\mu$ spectrum below 5 meV. Even though the low-lying peak structure grows in intensity and its peak position is shifted to the lower energy above H_c, the broad continuumlike absorption scarcely depends on H ($H_c \approx 20$ kOe at 7 K); the $E^\omega \| a$ polarized absorption is similarly identified as the most notable electric-dipole active band even in the ab spiral spin phase. Such a tendency is also seen in H dependence of N_{eff}, as shown in Fig. 6(b). We selected $\omega_1 = 0.7$ meV and $\omega_2 = 5$ meV to estimate N_{eff} of the low-lying excitation. The negligible effect of H is clearly discerned; even H exceeds H_c. This behavior is different from the reported result of TbMnO$_3$, in which the low-lying electromagnon disappears by application of H up to 80 kOe at 12 K (Ref. 10). In the experiment of Ref. 10, H was applied along the c axis, thus giving rise to the suppression of P_s along the c axis, according to the ME phase diagram of TbMnO$_3$.[4] Namely, the flop of P_s from along the c axis to the
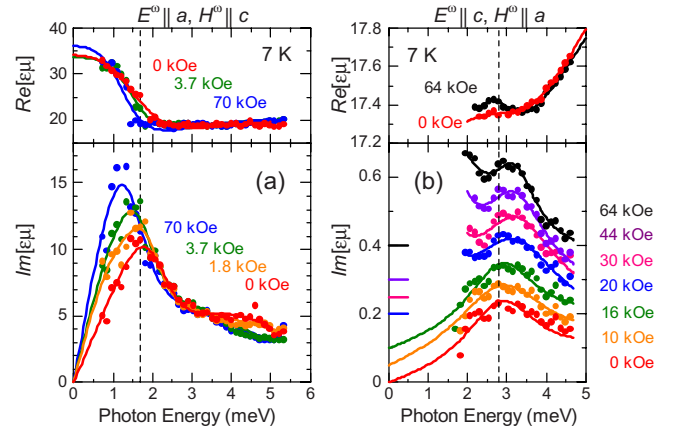

FIG. 5. (Color online) Magnetic-field (H) dependence of the real (upper panels) and imaginary (lower panels) parts of the selected $\epsilon\mu$ spectra (closed circles) of the ac surface crystal plate of DyMnO$_3$ at 7 K when (a) E^ω or (b) H^ω was set parallel to the a axis. The ferroelectric polarization flop occurs at 20 kOe for $H \| b$. Note that Im[$\epsilon\mu$] spectra in (b) are vertically offset for clarity and that the scale of the vertical axis is different in (a) and (b).

a axis or equivalently the rotation of the spiral spin plane from bc to ab cannot be induced unless the H is applied along the a or b axis, as we adopted here. In addition, we measured the $\epsilon\mu$ spectra for $E^\omega \| a$ at 17 K just below T_c in H along the b axis up to 70 kOe to confirm the same tendency. Furthermore, we gathered the $\epsilon\mu$ spectra for $E^\omega \| c$ and $H^\omega \| a$ at 7 K in H up to 70 kOe. The upper and lower panels of Fig.
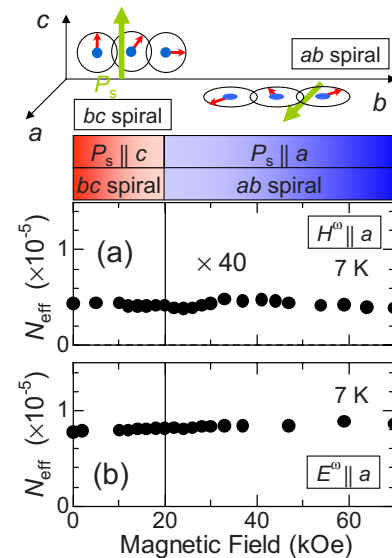

FIG. 6. (Color online) Magnetic-field (H) dependence of the integrated spectral weight per Mn-site, N_{eff}, as defined by Eq. (1) in the text of the ac surface crystal plate of DyMnO$_3$ for (a) $H^\omega \| a$ and (b) $E^\omega \| a$, measured at 7 K. The upper panel of (a) shows the phase diagram with variation of H. We also show the schematic illustrations of the bc and ab spiral spin planes induced by H. H of 20 kOe at which the ferroelectric polarization flop occurs at 7 K, is indicated by the vertical solid line in (a) and (b). The difference of N_{eff} at 7 K with [in (a) and (b)] and without H (in Fig. 4), arises from the difference of the integrated energy range (see text).

5(b) shows the selected Re[$\epsilon\mu$] and Im[$\epsilon\mu$] spectra, respectively. The estimated N_{eff} is also presented in Fig. 6(a) (we used $\omega_1 = 2.4$ meV and $\omega_2 = 4$ meV). Above H_c, the direction of E^ω ($\parallel c$) becomes perpendicular to the spiral spin plane and hence would activate the electromagnon arising from the rotational mode of the ab spiral spin plane. Even though the evolution of the tiny absorption is visible around 2 meV above H_c, the strong absorption, to be compared with Im[$\epsilon\mu$] for $E^\omega \parallel a$ in zero H, is not discerned at all for $E^\omega \parallel c$ but only for $E^\omega \parallel a$.

IV. DISCUSSION

In the spiral spin phase of RMnO$_3$, the electromagnon or equivalently the rotational mode of the spiral spin plane is expected to become active when E^ω is set perpendicular to the spiral spin plane, i.e., $E^\omega \parallel a$ and $E^\omega \parallel c$ in bc and ab spiral spin phases, respectively. This scenario is theoretically considered on the basis of the spin-current mechanism (Ref. 12) that is now recognized to explain the magnetically driven ferroelectricity in a variety of multiferroics found so far, including RMnO$_3$.[6] Indeed, a single peak structure around 2.5 meV has been identified in the ϵ spectrum for $E^\omega \parallel a$ in the bc spiral spin phase of TbMnO$_3$ (Ref. 10). Accordingly, one of the low-energy branches of the magnon band, i.e., around 2 meV at $k=0$, in the bc spiral spin phase of TbMnO$_3$ was assigned to be responsible for the electromagnon model by inelastic neutron-scattering experiments (Ref. 24).

In the present study, we could uncover new features of the low-energy spin excitation driven by either E^ω or H^ω in a variety of spin phases of DyMnO$_3$ on the basis of the detailed light-polarization, T, and H dependences, as presented in Sec. III. First, our result can provide the compelling evidence that the possibility of the rotational mode of the spiral spin plane is excluded as the origin of the intense absorption around 2–3 meV for $E^\omega \parallel a$, which is also observed in the bc spiral spin phase of TbMnO$_3$.[10] We firmly identify that the electric-dipole active spin excitation along the a axis well survives even in the ab spiral spin phase induced by applying H up to 70 kOe along the b axis [Fig. 5(a)]. This observation clearly contradicts the former theoretical[12] and experimental[24] arguments described above. Second, we clarify that the electric-dipole active spin excitation along the a axis can be regarded as the continuumlike absorption band with two broad peak structures (1–8 meV) [Figs. 2(a) and 2(b)] rather than the single peak structure (1–5 meV) as reported in the bc spiral spin phase of TbMnO$_3$ (Ref. 10). Third, we identify the spin excitation with a single peak structure when H^ω is set parallel to the a axis or the c axis [Figs. 2(d)–2(f)], which can be assigned to the antiferromagnetic resonance (AFMR) of Mn spins at $k=0$. The $k=0$ magnon mode for $H^\omega \parallel a$ can be reasonably ascribed to one of the lower branches of the magnon, as observed around 2 meV at $k=0$ in the inelastic neutron-scattering spectrum of the bc spiral spin phase of TbMnO$_3$, even though it was previously assigned to the rotational mode of the spiral spin plane.[24] This complexity partly comes from the fact that the peak position of AFMR for $H^\omega \parallel a$ nearly matches the peak position of the low-lying peak structure for $E^\omega \parallel a$ as we revealed here [Figs. 2(a) and 2(d)]. On the contrary, the observed

broad continuumlike band for $E^\omega \parallel a$ spreads over the wide energy range (1–10 meV), which cannot be explained by $k=0$ magnon absorption alone.

The observed broad peak and continuumlike (0–10 meV) shape of the electric-dipole active band does suggest that the spin fluctuation related to the excitation such as the two-magnon is more plausible rather than the Goldstone mode-like electromagnon. The optically active two-magnon excitations are possible over the full magnon bandwidth with the combination of $+k$ and $-k$ magnons and hence should distribute the spectral weight up to the energy twice of the magnon bandwidth. According to the inelastic neutron-scattering study on TbMnO$_3$ (Refs. 23 and 24), the magnon bandwidth is about 8 meV. This value is considerably narrowed as compared with that of LaMnO$_3$ ($\sim$32 meV) (Ref. 27) or PrMnO$_3$ ($\sim$20 meV) (Ref. 23) with the A-type antiferromagnetic ground state due to the larger orthorhombic lattice distortion as well as to the strong spin frustration effect in the cycloidal magnet TbMnO$_3$. The magnon bandwidth of DyMnO$_3$, in which the inelastic neutron-scattering study would be difficult to perform due to the presence of the neutron-absorbing Dy ions, should be comparable to or slightly smaller than that of TbMnO$_3$ since DyMnO$_3$ is structurally close to TbMnO$_3$ and shows the similar bc plane cycloidal order at the ground state.[4] Therefore, two-magnon energy range is anticipated to be up to 10–15 meV, which well fits the observed energy range of the electric-dipole active spin excitations.

Here we propose that the observed unique optical dipole activity may share the same origin, i.e., the spin-current mechanism,[6] with the static P_s. The strong $E^\omega \parallel a$ selection rule irrespective of the bc or ab spiral spin plane does suggest the large mutual fluctuation within the ac plane of the neighboring spins lining up along the c axis but not along the b nor a axis; namely, $(\delta S_i \times \delta S_j) \parallel b$, $e_{ij} \parallel c$, and hence δP^ω $[\propto e_{ij} \times (\delta S_i \times \delta S_j)] \parallel a$. The antiferromagnetic exchange interaction along the c axis in the perovskite manganite is likely the origin of the large spin fluctuation contrary to the ferromagnetic coupling along the a axis. This scenario, although a more elaborate theory is needed, may qualitatively explain the strong optical activity for $E^\omega \parallel a$ also in the spin-collinear paraelectric phase as observed. Then, broad peaks around 2 and 5.5 meV may be assigned to the density-of-state singularities of the two-magnon band.

V. SUMMARY

In summary, we have measured the $\epsilon\mu$ spectra of a complete set of possible configurations of single crystals of DyMnO$_3$ by using terahertz time-domain spectroscopy. A rich variety of optical excitation at terahertz frequencies was identified by detailed measurements of light-polarization, T, and H dependences. In particular, the spin excitation driven by E^ω was confirmed to become strongly electric-dipole active along the a axis, irrespective of the bc or ab spiral spin plane. The broad (1–10 meV) band feature indicates the contribution of two-magnon-like excitations arising from the large fluctuations of spin and spin-current inherent to this spiral magnet.
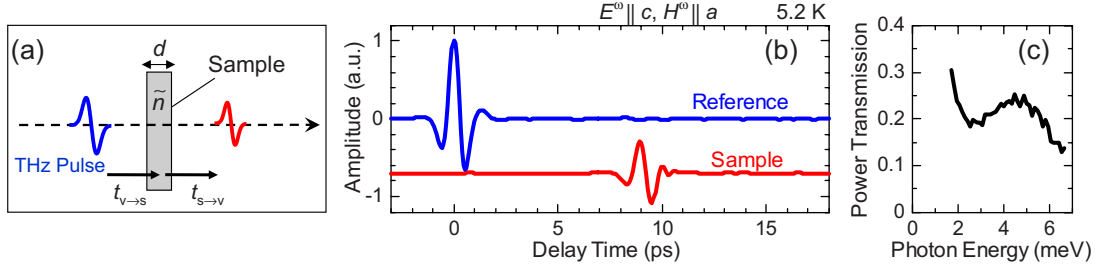
FIG. 7. (Color online) (a) Sample geometry with the complex Fresnel transmission coefficients from vacuum to the sample $t_{v \to s}$ and from the sample to vacuum $t_{s \to v}$. The complex transmission coefficient t was obtained by Eq. (B1). d and $\tilde{n}$ are the thickness and the complex refractive index of the sample, respectively. (b) Typical example of the measured terahertz wave form in time-domain with and without the sample (ac surface crystal plate of $DyMnO_3$) measured at 5.2 K in zero magnetic field. E^{ω} and H^{ω} were set parallel to the c and a axes, respectively. The amplitude of the transmitted terahertz wave form with the sample was vertically offset for clarity. (c) Power transmission spectrum of $DyMnO_3$.

APPENDIX A: RAW DATA OF TERAHERTZ RADIATION IN TIME DOMAIN

A unique advantage for the use of terahertz time-domain spectroscopy is to directly monitor the electric field of the radiated terahertz pulse in time domain.[28] This technique yields the amplitude and phase spectra by the fast Fourier transformation (FFT) of the measured terahertz wave forms with and without the sample. Therefore, we need no KK transformation, which is necessary for obtaining the complex optical spectra by conventional optical spectroscopy. As a typical example, we show in Fig. 7(b) the transmitted terahertz wave form with the sample in time-domain performed at 5.2 K in zero H. The sample was the ac surface crystal plate of $DyMnO_3$. E^{ω} and H^{ω} were set parallel to the c and a axes, respectively. We also plotted the reference of terahertz pulse used in this setup. The amplitude of the transmitted terahertz wave form is reduced due to the absorption of the sample, as compared to the reference. Its phase is also delayed due to the refractive index of the sample. The ratio between FFT spectrum with and without the sample,

$$\frac{E_{sample}}{E_{ref}} \equiv \sqrt{\mathcal{T}} \exp(-i\phi) \qquad (A1)$$

can yield the power transmission $\mathcal{T}$ and phase ϕ spectra. The example of the obtained $\mathcal{T}$ spectrum is shown in Fig. 7(c). We can identify the clear absorption peak structure around 3 meV. This peak can be assigned to the spin excitation driven by $H^{\omega} \| a$, as presented in Fig. 2.

APPENDIX B: RELATIONSHIP BETWEEN TRANSMISSION COEFFICIENT AND OPTICAL CONSTANTS

We numerically derived the complex optical spectra without the KK transformation by adopting the following procedure. Without taking into account the effect of the multiple reflections inside the sample, the complex transmission coefficient t for bulk in normal incidence as schematically shown in Fig. 7(a) can be simply expressed as

$$t = t_{v \to s} t_{s \to v} \exp\left(-i\frac{\omega}{c}d(\tilde{n} - 1)\right) = \frac{E_{sample}}{E_{ref}}, \qquad (B1)$$

where ω is the frequency, c the velocity of light, d the thickness of the sample, and $\tilde{n}$ ($= n + i\kappa$) the complex refractive index of the sample.[29] Experimentally, the effect of the multiple reflections can be avoided by restricting the time range of the FFT. The complex Fresnel transmission coefficients[29] from vacuum to the sample $t_{v \to s}$ and from the sample to vacuum $t_{s \to v}$ can be, respectively, given by

$$t_{v \to s} = \frac{2}{\tilde{n} + 1}, \qquad (B2a)$$

$$t_{s \to v} = \frac{2\tilde{n}}{\tilde{n} + 1}, \qquad (B2b)$$

when the complex magnetic permeability μ is 1. In this case, $\tilde{n}$ can be expressed as $\sqrt{\epsilon}$, where ϵ is the complex dielectric constant of the sample. Accordingly, $\tilde{n}$ and thus ϵ can be numerically calculated from Eq. (B1) using experimentally determined values; $\mathcal{T}$ and ϕ in Eq. (A1). This procedure is widely recognized to estimate $\tilde{n}$ and ϵ of a variety of materials including dielectrics, semiconductors, and metals.[16,18]

On the contrary, in magnetic materials, $\tilde{n}$ should be exactly expressed as $\sqrt{\epsilon\mu}$ near the magnetic resonance, which usually locates around $\sim$meV (Ref. 30). In this case, Eqs. (B2a) and (B2b) should be, respectively, replaced by

$$t_{v \to s} = \frac{2\mu}{\tilde{n} + \mu}, \qquad (B3a)$$

$$t_{s \to v} = \frac{2\tilde{n}}{\tilde{n} + \mu}. \qquad (B3b)$$

APPENDIX C: ESTIMATION PROCEDURE OF COMPLEX OPTICAL SPECTRA

In the cases of the measurements for $E^\omega \| a$ using ac and ab surface crystal plates of DyMnO$_3$, we experimentally identified from light-polarization dependences [Figs. 2(a) and 2(b)] that the observed large absorption originates from E^ω response. The H^ω response in these configurations can be considered to be negligible compared to E^ω response. This is confirmed from the results using bc surface crystal plate where there is no absorption in $H^\omega \| b$ ($E^\omega \| c$) [Fig. 2(c)] and only a slight absorption in $H^\omega \| c$ ($E^\omega \| b$) [Fig. 2(f)]. Therefore, we assume $\mu = 1$ in the Fresnel coefficient and used Eqs. (B2a) and (B2b) while keeping $n = \sqrt{\epsilon\mu}$ in Eq. (B1) for generality. This is also applied to the case for $E^\omega \| c$ and $H^\omega \| b$, in which the negligible absorption is clearly identified [Fig. 2(c)]. We numerically solved Eq. (B1) combined with Eqs. (B2a) and (B2b) to match the measured values given by Eq. (A1) and determined the $\epsilon\mu$ spectra. For the sake of convenience, we used the quantities of Re[$\epsilon\mu$] and Im[$\epsilon\mu$] in this paper although they can be precisely expressed as Re[ϵ] and Im[ϵ] in the above condition.

On the other hand, we identify a peak structure around 3 meV, which only appears when H^ω was set parallel to the a axis [Figs. 2(d) and 2(e)] or the c axis [Fig. 2(f)]. These small absorption can be assigned to H^ω response. In addition, a broad background absorption is observed above 4 meV as seen in the power transmission spectrum at 5.2 K [Fig. 7(c)], which can be attributed to the tail of the optical phonon lying around 16 meV.[13] In such a case, both ϵ and μ could contribute to the transmission spectrum. Accordingly, four independent quantities, Re[ϵ], Im[ϵ], Re[μ], and Im[μ], cannot be obtained only from the transmission measurements of $\mathcal{T}$ and ϕ. However, in the case of a thick sample, the main signature of the transmission spectrum is dominated by bulk absorption and the effect of μ in the Fresnel coefficient is considered to be small as discussed below. Therefore, we used the Fresnel coefficient of Eqs. (B2a) and (B2b), while the effect of H^ω response was taken into account by adopting $\tilde{n} = \sqrt{\epsilon\mu}$ in Eq. (B1). The validity of this approach was firmly confirmed following calculation.

We numerically solved Eq. (B1) by putting Eqs. (B3a) and (B3b) with Re[μ] and Im[μ] as fixed parameters with respect to ω and estimated Im[$\epsilon\mu$] spectra of DyMnO$_3$ for $E^\omega \| c$ and $H^\omega \| a$ at 5.2 K. For examples, we show in Fig. 8(a) the calculated Im[$\epsilon\mu$] spectra at selected values of Re[μ] and Im[μ]. The fixed parameters used here are provided in the right-hand side of the figure. The Im[$\epsilon\mu$] spectrum, as derived from Eqs. (B2a) and (B2b) {Re[μ]=1 and Im[μ]=0 in Eqs. (B3a) and (B3b)}, is also plotted by closed circles with a solid line. As can be clearly seen in the figure, no significant difference is observed even though μ is included to $t_{v \to s}$ and $t_{s \to v}$.

To further check the validity of the used values of Re[μ] and Im[μ], we assumed that ϵ comes from the contribution
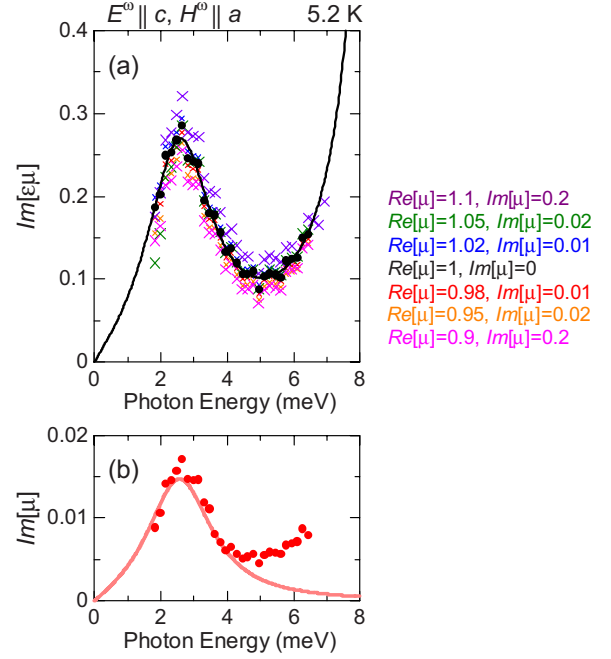

FIG. 8. (Color online) (a) Validity of using Eqs. (B2a) and (B2b) instead of Eqs. (B3a) and (B3b). The Im[$\epsilon\mu$] spectra of DyMnO$_3$ for $E^\omega \| c$ and $H^\omega \| a$ at 5.2 K was almost unchanged even if we used Eqs. (B3a) and (B3b). The fixed parameters of Re[μ] and Im[μ] are described in the right-hand side of the figure, which were confirmed to be reasonable by assuming that ϵ can be represented by a single Lorentz oscillator [see (b)]. (b) The estimated Im[μ] spectrum (closed circles) by assuming that ϵ can be represented by a single Lorentz oscillator. We also plot the Im[μ] spectrum (a solid line) as extracted from Eq. (B1) combined with Eqs. (B2a) and (B2b).

of the optical-phonon structure, which can be represented by a single Lorentz oscillator. This approximation has been conventionally used to estimate the μ spectra in antiferromagnets as exemplified by the cases of the orthoferrites.[30] We used the following parameters: the resonance frequency, the damping rate, and the dielectric constant for the high frequency above the measured range were set to 9 meV, 0.5 meV, and 16 meV, respectively. With this approximation, the Im[μ] spectrum was numerically calculated using Eq. (B1) combined with Eqs. (B3a) and (B3b). The result is presented in Fig. 8(b) by closed circles. We also show the Im[μ] spectrum (a solid line) as derived from the Im[$\epsilon\mu$] spectrum that was estimated by using Eqs. (B2a) and (B2b). We assumed that the Im[$\epsilon\mu$] spectrum (=Re[ϵ]Im[μ]+Im[ϵ]Re[μ]) can be expressed by two Lorentz oscillators for ϵ and μ. Both data coincide with each other below 4 meV, ensuring the validity of using Eqs. (B2a) and (B2b). Noticeably, the maximum values of Re[μ] and Im[μ] are estimated to be about 1.01 and 0.02, respectively, indicating that the fixed parameters shown in Fig. 8(a) are reasonable. However, there is a discrepancy above 4 meV, which mainly arises from the lack of the spectral information above 6 meV and thus from the inappropriate parameters used here to reproduce the optical-phonon structure. In this work, we numerically solved using Eq. (B1) with Eqs. (B2a) and (B2b) and estimated $\tilde{n}$ ($=\sqrt{\epsilon\mu}$) spectra.

[1] For recent reviews of multiferroics, Y. Tokura, Science **312**, 1481 (2006); W. Eerenstein, N. D. Mathur, and J. F. Scott, Nature (London) **442**, 759 (2006); S.-W. Cheong and M. Mostovoy, Nat. Mater. **6**, 13 (2007); Y. Tokura, J. Magn. Magn. Mater. **310**, 1145 (2007).

[2] T. Kimura, T. Goto, H. Shintani, K. Ishizaka, T. Arima, and Y. Tokura, Nature (London) **426**, 55 (2003).

[3] T. Goto, T. Kimura, G. Lawes, A. P. Ramirez, and Y. Tokura, Phys. Rev. Lett. **92**, 257201 (2004).

[4] T. Kimura, G. Lawes, T. Goto, Y. Tokura, and A. P. Ramirez, Phys. Rev. B **71**, 224425 (2005).

[5] M. Kenzelmann, A. B. Harris, S. Jonas, C. Broholm, J. Schefer, S. B. Kim, C. L. Zhang, S.-W. Cheong, O. P. Vajk, and J. W. Lynn, Phys. Rev. Lett. **95**, 087206 (2005).

[6] H. Katsura, N. Nagaosa, and A. V. Balatsky, Phys. Rev. Lett. **95**, 057205 (2005).

[7] I. A. Sergienko and E. Dagotto, Phys. Rev. B **73**, 094434 (2006).

[8] M. Mostovoy, Phys. Rev. Lett. **96**, 067601 (2006).

[9] Y. Yamasaki, H. Sagayama, T. Goto, M. Matsuura, K. Hirota, T. Arima, and Y. Tokura, Phys. Rev. Lett. **98**, 147204 (2007).

[10] A. Pimenov, A. A. Mukhin, V. Yu. Ivanov, V. D. Travkin, A. M. Balbashov, and A. Loidl, Nat. Phys. **2**, 97 (2006).

[11] G. A. Smolenski and I. E. Chupis, Usp. Fiziol. Nauk **137**, 415 (1982) [Sov. Phys. Usp. **25**, 475 (1982)].

[12] H. Katsura, A. V. Balatsky, and N. Nagaosa, Phys. Rev. Lett. **98**, 027203 (2007).

[13] A. Pimenov, T. Rudolf, F. Mayr, A. Loidl, A. A. Mukhin, and A. M. Balbashov, Phys. Rev. B **74**, 100403(R) (2006).

[14] R. Valdés Aguilar, A. B. Sushkov, C. L. Zhang, Y. J. Choi, S. W. Cheong, and H. D. Drew, Phys. Rev. B **76**, 060404(R) (2007).

[15] A. Pimenov, A. Loidl, A. A. Mukhin, V. D. Travkin, V. Yu. Ivanov, and A. M. Balbashov, Phys. Rev. B **77**, 014438 (2008).

[16] For reviews of tetrahertz time-domain spectroscopy, M. C. Nuss and J. Orenstein, *Millimeter and Submillimeter Wave Spectroscopy of Solids*, edited by G. Grüner (Springer, Berlin, 1998), pp. 7–50; C. A. Schmuttenmaer, Chem. Rev. (Washington, D.C.) **104**, 1759 (2004).

[17] For a recent review of THz technology, M. Tonouchi, Nat. Photonics **1**, 97 (2007).

[18] For a recent review of PC sampling technique, *Terahertz Optoelectronics*, edited by K. Sakai (Springer, Berlin, 2005).

[19] Q. Wu and X.-C. Zhang, Appl. Phys. Lett. **71**, 1285 (1997).

[20] K. Yang, P. L. Richards, and Y. R. Shen, Appl. Phys. Lett. **19**, 320 (1971).

[21] D. H. Auston, K. P. Cheung, and P. R. Smith, Appl. Phys. Lett. **45**, 284 (1984).

[22] Y. Ikebe and R. Shimano, Appl. Phys. Lett. **92**, 012111 (2008).

[23] R. Kajimoto, H. Mochizuki, H. Yoshizawa, H. Shintani, T. Kimura, and Y. Tokura, J. Phys. Soc. Jpn. **74**, 2430 (2005).

[24] D. Senff, P. Link, K. Hradil, A. Hiess, L. P. Regnault, Y. Sidis, N. Aliouane, D. N. Argyriou, and M. Braden, Phys. Rev. Lett. **98**, 137206 (2007).

[25] J. Strempfer, B. Bohnenbuck, M. Mostovoy, N. Aliouane, D. N. Argyriou, F. Schrettle, J. Hemberger, A. Krimmel, and M. v. Zimmermann, Phys. Rev. B **75**, 212402 (2007).

[26] T. Arima, T. Goto, Y. Yamasaki, S. Miyasaka, K. Ishii, M. Tsubota, T. Inami, Y. Murakami, and Y. Tokura, Phys. Rev. B **72**, 100102(R) (2005).

[27] K. Hirota, N. Kaneko, A. Nishizawa, and Y. Endoh, J. Phys. Soc. Jpn. **65**, 3736 (1996).

[28] D. Grischkowsky, S. Keiding, M. van Exter, and C. Fattinger, J. Opt. Soc. Am. B **7**, 2006 (1990).

[29] M. Born and E. Wolf, *Principles of Optics* (Pergamon, New York, 1975).

[30] A. M. Balbashov, G. V. Kozlov, A. A. Mukhin, and A. S. Prokhorov, in *High Frequency Processes in Magnetic Materials*, edited by G. Srinivasan and A. N. Slavin (World Scientific, Singapore, 1995), pp. 56–98.